Solar Cells, *31* (1991) 259–278

The influence of spectral solar irradiance variations on the performance of selected single-junction and multijunction solar cells

P. Faine, Sarah R. Kurtz, C. Riordan and **J. M. Olson**
Solar Energy Research Institute, 1617 Cole Blvd., Golden, CO 80401 (U.S.A.)

(Received November 20, 1990)

Abstract

The sensitivities of selected single-junction and multijunction cells to variations in solar irradiance are presented. The one-sun spectral irradiance is varied as a function of air mass, optical aerosol depth (turbidity) and amount of precipitable water vapor for direct-normal and global-normal geometries. Several devices, including one-, two- and three-junction devices with low and high bandgaps and either series- or independent-connection schemes, were investigated. The effects of air mass and turbidity on the consistency of high-bandgap device performance are shown to be greater than the effect of precipitable water vapor. Low-bandgap devices are less affected by variations in air mass and turbidity, but are more sensitive to high water-vapor conditions. The efficiency gained by redesigning a multijunction device for the latitude at which it is expected to be used is shown to be less than about 3% (relative).

1. Introduction

Commonly used solar spectral irradiance data for reporting and comparing solar cell performances are the air mass (AM) 1.5 spectra adopted as standards by the American Society for Testing and Materials (ASTM) [1, 2]. These AM 1.5 spectra were generated using a spectral irradiance model and a single set of atmospheric and sun-angle conditions (*e.g.* 1.42 cm of precipitable water vapor, sea-level surface pressure and 48.19° solar zenith angle) [3]. Because spectral irradiance varies with different atmospheric and sun-angle conditions (*i.e.* different climates and locations), questions arise as to whether the AM 1.5 performance results are representative and how sensitive different single-junction and multijunction cells are to outdoor (terrestrial) spectral irradiance variations. Questions about sensitivity to spectral solar irradiance variations, outdoor performance and optimum design have been addressed in other studies [4] for specific solar cells and solar irradiance conditions. However, the results of these other studies cannot easily be extrapolated to any solar cell because the results depend on solar cell characteristics, the models used to characterize their performance and the range of spectral irradiance conditions represented in the studies.

In this report, we use a simple spectral irradiance model (SPCTRAL2 [5]) and a simple solar cell model [6] to examine the influence of particular

0379-6779/91/$3.50

cloudless-sky spectral irradiance variations on the performance of a selected set of single-junction and multijunction solar cells at one sun and 27 °C. The objectives are to show the influence of solar spectral irradiance variations on the performance and optimum design of these solar cells and to determine whether these variations in performance differ substantially for multijunction and single-junction cells. This report supplements a less detailed study, which considers the effect of cell temperature and spectral fluctuations on the efficiencies of selected one-, two- and three-junction cells with various connection schemes at 100 X concentration [7].

2. Methods

2.1. Solar spectral irradiance

2.1.1. Important variables

The variables that have the largest effect on spectral irradiance variations are air mass (calculated from sun angle), clouds, turbidity (aerosol effects), precipitable water vapor and, to a lesser extent, surface pressure, ground reflectance and amount of ozone. These are generally the parameters which are varied, with different levels of detail and complexity, in models to predict spectral irradiance. In addition, the solar radiation components (direct-beam or global (direct-beam plus diffuse)) used by a solar cell (concentrator or flat-plate) must be characterized separately because these components have different spectral distributions. The effects of these variables on spectral irradiance are as follows.

The total irradiance available to flat-plate photovoltaic (PV) systems is loosely termed global irradiance. Global irradiance is composed of direct-beam solar radiation from the sun's disk, diffuse (scattered) radiation from the sky and ground-reflected radiation. If a PV system is sun-tracking, the direct beam is normal to the PV system's surface; otherwise the direct-beam component is reduced by the cosine of the incidence angle. The total irradiance available to a sun-tracking flat-plate PV system is loosely called "global normal", and the irradiance available to a sun-tracking concentrator PV system is called direct normal. The two ASTM AM 1.5 standard spectra were modeled for a direct-normal case and for a global case where the collector surface is south-facing and tilted 37° from the horizontal (the direct-beam incidence angle is 11.2° for this case).

AM refers to the relative path length of the solar beam through the atmosphere and depends on the angle of the sun from the vertical (solar zenith angle) or from the horizon (solar elevation). AM is 1.0 when the sun is directly overhead, 1.5 when the sun is 48.2° from the vertical and 2.0 when the sun is at 60°. The two ASTM AM 1.5 standard spectra therefore represent the case where the solar zenith angle is 48.2°. Because the collector surface for the global case is south-facing at a 37° tilt, the incidence angle is 48.2° minus 37°, or 11.2°.

AM is important because with longer path lengths (higher AM values) there is more opportunity for scattering and absorption of solar radiation

(attenuation) by atmospheric constituents, such as clouds, aerosols and water vapor (Fig. 1). Sun angles vary with latitude, time of the day and day of the year. Therefore latitude, time and day of the year are varied in the calculations shown later to account for AM effects.

In this report, we consider only cloudless-sky conditions as a first approximation of the influence of spectral irradiance variations on solar cells. The ASTM AM 1.5 spectra also represent cloudless-sky conditions. The spectral effects of clouds are under investigation [8, 9], but they are not considered in the results presented here.

Atmospheric aerosol optical depth (or turbidity) is a measure of the atmospheric attenuation of solar radiation by aerosols. It is a dimensionless quantity, with a value of 0.1 (at 0.5 μm) indicating a relatively clear atmosphere and a value of 0.4 indicating a relatively turbid atmosphere. The ASTM AM 1.5 standard spectra were calculated using a rural aerosol model and a turbidity value of 0.27 at 0.5 μm [3]. The spectral effects of aerosol attenuation depend on the properties of the aerosols, such as size relative to the wavelength of solar irradiance, but the effects generally increase with decreasing wavelength (Fig. 2) and are larger for direct compared with global irradiance.

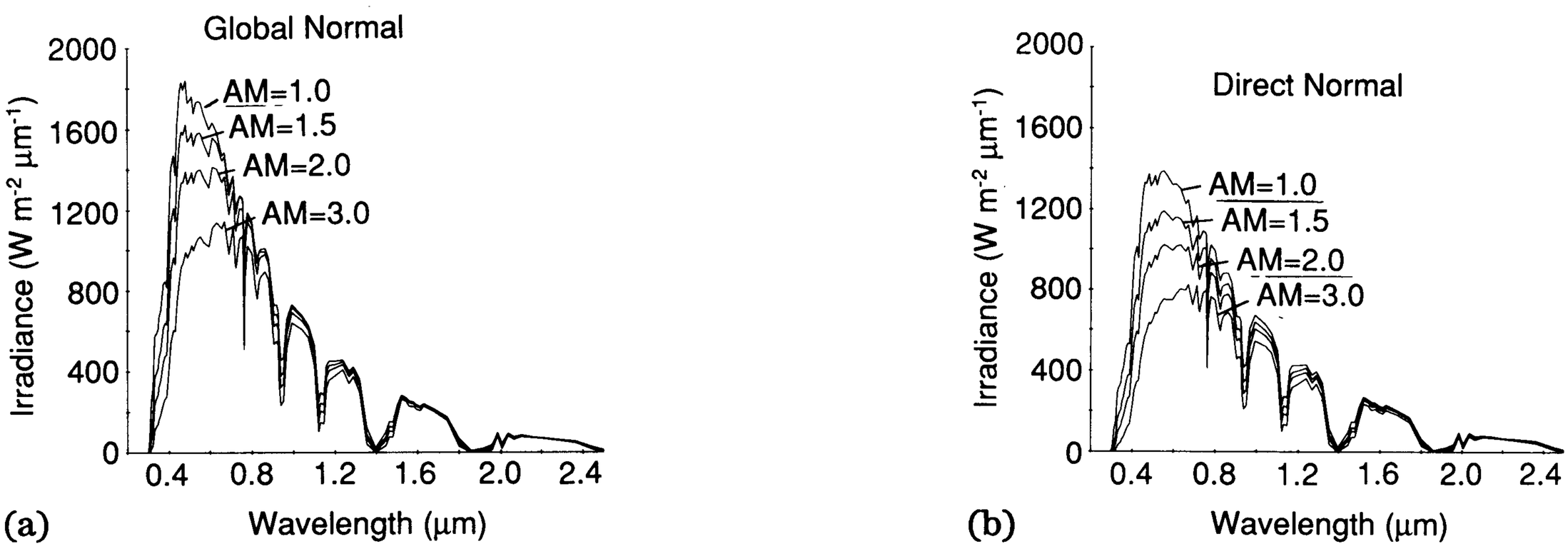

Fig. 1. Variation of simulated [5] global-normal (a) and direct-normal (b) spectral solar irradiance with increasing air mass (AM), with other variables held constant.

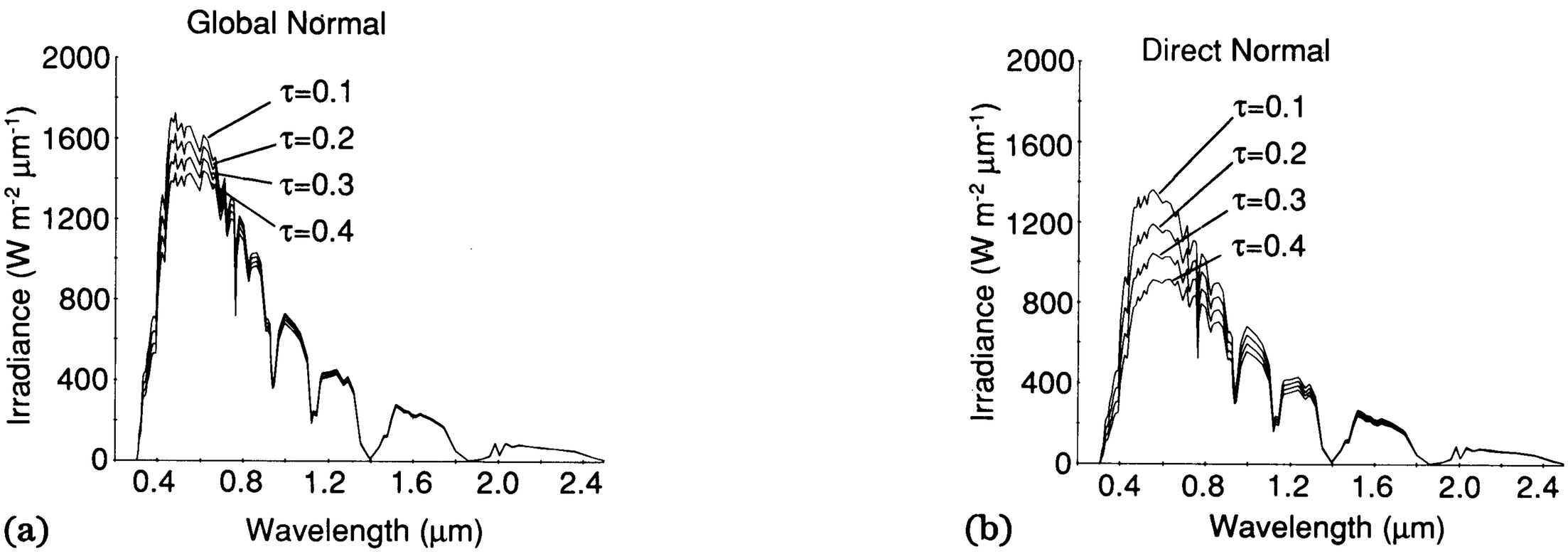

Fig. 2. Variation of simulated [5] global-normal (a) and direct-normal (b) spectral solar irradiance with increasing turbidity (τ), with other variables held constant.

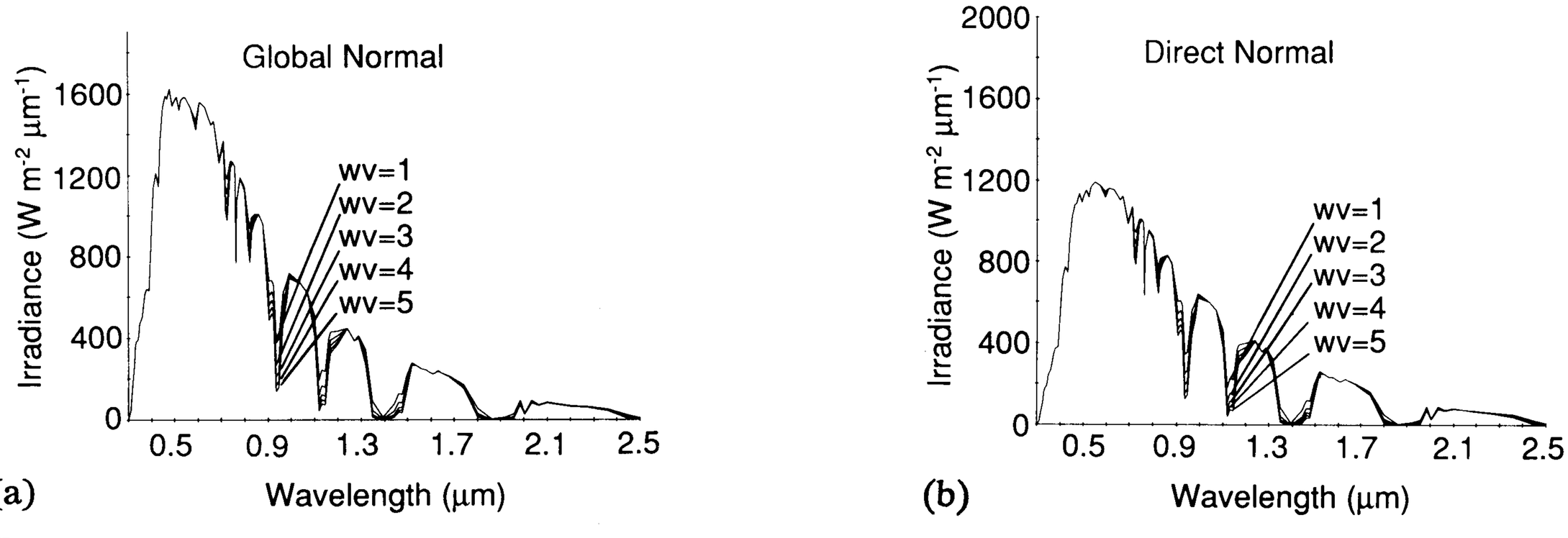

Fig. 3. Variation of simulated [5] global-normal (a) and direct-normal (b) spectral solar irradiance with increasing precipitable water vapor (wv), with other variables held constant.

Precipitable water vapor causes absorption of solar radiation in absorption bands shown in Fig. 3. As water vapor increases, the absorption regions deepen and broaden (unless they are saturated). A precipitable water-vapor value of about 1 cm is representative of a relatively dry atmosphere, and a value of about 5 cm is representative of a relatively wet atmosphere. The precipitable water-vapor value corresponding to the ASTM AM 1.5 standard spectra is 1.42 cm [3].

Surface pressure, which mostly depends on site elevation, is related to the number of air molecules in the atmospheric path between the sun and the earth's surface. The path length (or AM) is pressure-corrected in calculations of molecular (Rayleigh) scattering to account for decreased density with higher elevations. Rayleigh scattering has a strong spectral dependence that increases with decreasing wavelength. The ASTM AM 1.5 standard spectra were modeled for sea-level surface pressure (1013 mbar) [3].

Ground reflectance influences the amount of radiation reflected between the ground and air and the amount of radiation reflected from the ground onto a surface tilted from the horizontal. Spectral ground reflectance can vary widely, but the effects on total spectral irradiance are relatively small for cloudless-sky conditions, except for cases of high-albedo ground surfaces (such as snow) and tilted surfaces. A constant spectral ground albedo of 0.2 (representing an average value for dry bare soil) was used in generating the ASTM AM 1.5 standard spectra [3] and in all calculations reported here.

Ozone is a strong absorber in the UV region of the spectrum (below 0.35 μm) and, to a lesser extent, in the visible region. Typical seasonal and latitude variations of ozone cause spectral variations that are relatively minor in the wavelengths important to solar cell performance.

2.1.2. The spectral irradiance model

Spectral irradiance is calculated using a simple cloudless-sky irradiance model called SPCTRAL2. It was developed using comparisons with more complex models and limited outdoor measurements. SPCTRAL2 calculates irradiance at 122 wavelengths that were selected to minimize the number of wavelength calculations, while retaining the major structure in the spectrum.

Input to the model includes latitude, longitude, day of the year, solar zenith angle, aerosol optical depth at 0.5 μm (turbidity), precipitable water vapor, surface pressure, ground reflectance and irradiance component (*e.g.* direct or global). A subroutine called SOLPOS was used to compute solar zenith angle as a function of latitude, day of the year and time of day. Latitude, longitude and day of the year are used to calculate the amount of ozone, which varies with location and time of year (day of the year or day number).

There are a large number of possible combinations of these variables, and so for practical (computation) reasons, only one or two of them are varied while others (such as ground reflectance and surface pressure) are held constant. For the results reported here, AM was varied from 1.0 to 11.5, turbidity from 0.1 to 0.4 and precipitable water vapor from 1 to 5 cm. The surface pressure was always set for sea level or 1580 m elevation for Golden, CO; the ground reflectance was set to 0.2 for all wavelengths, the latitude was varied from 0° to 70° and all times of the day and year were considered.

2.2. Solar cell performance model

A detailed description of the calculation method has been presented elsewhere [6] and is similar to the methods used by Fan *et al.* [10], Nell and Barnett [11] and Wanlass *et al.* [12]. The one-sun short-circuit photocurrent J_L of each junction (subcell) was calculated from

$$J_L = \sum_{\lambda} eI_0(\lambda)\Delta\lambda[1-\exp\{-\alpha(\lambda)t\}] \tag{1}$$

where e is the electronic charge, $I_0(\lambda)$ is the intensity incident on the subcell as a function of wavelength λ, $\alpha(\lambda)$ is the spectral absorption coefficient of the subcell material and t is the thickness of the subcell. Thus a quantum efficiency of unity was assumed (*i.e.* no reflection, grid or surface recombination losses). In all cases, the bottom cell was assumed to be infinitely thick. The reverse-saturation current J_0 was calculated from material parameters [6] for each subcell using

$$J_0 = en_i^2\left[\left(\frac{D_e}{\tau_e}\right)^{1/2}\frac{\tanh\{\chi_p/(D_e\tau_e)^{1/2}\}}{N_A} + \left(\frac{D_n}{\tau_n}\right)^{1/2}\frac{\tanh\{\chi_n/(D_n\tau_n)^{1/2}\}}{N_D}\right] \tag{2}$$

where n_i is the intrinsic carrier concentration, N_A and N_D are the acceptor and donor concentrations, taken to be 10^{17} cm^{-3} and 2×10^{18} cm^{-3} respectively, χ_p and χ_n are the thicknesses of the p- and n-type layers respectively, D_e and D_n are the diffusion constants for electrons and holes respectively and τ_e and τ_n are the minority-carrier lifetimes of the electrons and holes respectively. The thickness χ_n of the emitter layer was 0.1 μm, while the thickness χ_p of the absorber layer was varied to optimize the efficiency of the cell, as described below. For the thickest cells, the dark currents were 2×10^{-23}, 2×10^{-16} and 1.4×10^{-2} mA cm^{-2} for the materials with bandgaps of 1.90, 1.424 and 0.6 eV respectively.

The maximum-power current of a series-connected two-terminal multijunction device is obtained by satisfying the condition

$$\left(\frac{\partial P}{\partial J}\right)=0 \tag{3}$$

where P is the multijunction-cell power and J is the multijunction-cell current (contrary to our statement in a previous paper [6], this is the same method as used by Nell and Barnett [11] and Wanlass *et al.* [12]). This calculation is equivalent to finding the multijunction-cell current J for which the following equation is satisfied

$$\sum_j \ln\left(\frac{J+J_{Lj}}{J_{0j}}\right)+J\times\sum_j\left(\frac{1}{J+J_{Lj}}\right)=0 \tag{4}$$

where j is the number of junctions (1–3) and J_{0j} and J_{Lj} are the reverse-saturation and light-generated currents respectively of the junction j. The solution J is then the multijunction-cell current at the maximum-power point. The power of each subcell is the product of J and V_j, where V_j is the subcell voltage calculated from the cell current J and the subcell reverse-saturation current J_{0j} using the diode equation, with a diode factor of unity and cell temperature of 27 °C. The power output of the four-terminal device is calculated using eqns. (1)–(3) on each subcell. The multijunction-cell power output is then the sum of the subcell powers.

The six types of single-junction (SJ) and multijunction (MJ) solar cells considered are given in Table 1.

We have shown previously that the efficiency of a series-connected MJ cell can be improved by thinning the top cell for cases in which the top-cell current is greater than the bottom-cell current(s) [6]. Here we have adjusted the top-cell thicknesses until the top- and bottom-cell short-circuit currents are equal for an AM 1.5 spectrum with turbidity of 0.2, water-vapor amount of 1 cm, albedo of 0.2 for all wavelengths and an elevation of

TABLE 1

Descriptions of the devices studied

Designation	Number of junctions (J)	Number of terminals (T)	Connection	Bandgap (E_g) (eV)
1J-HE_g	1	2	–	1.424
2J-2T-HE_g	2	2	Series	1.424/1.90
2J-2T-LE_g	2	2	Series	0.6/1.424
2J-4T-HE_g	2	4	Independent	1.424/1.90
2J-4T-LE_g	2	4	Independent	0.6/1.424
3J-2T	3	2	Series	0.6/1.424/1.90

HE_g, high bandgap; LE_g, low bandgap.

1580 m. Two different top-cell thicknesses were used for the direct- and global-normal results. In a few cases, we used slightly different devices. These are noted in the text.

2.3. Air-mass density function

An AM density function was derived so that annual and seasonal AM effects could be examined more efficiently than by calculating a solar spectrum and solar cell output at small increments of time on each day of the year. The following steps in the algorithm were used to derive the AM density function.

(i) SOLPOS was used to calculate the AM number for 280 points on each day of the year from sunrise time plus 30 min to sunset time minus 30 min for a particular location (longitude and latitude).

(ii) The amount of time spent at a particular AM value (0.05 AM intervals) was summed for the year or season to obtain the annual or seasonal AM density $f(a)$ for the specific location, where $f(a)$ is the number of hours during the year or season for which AM a is observed.

This algorithm was used to produce annual and seasonal AM density functions in hours per 0.05 AM intervals for several latitudes. The integrated annual efficiency η_{An} and power output of the solar cell are then calculated as follows

$$\eta_{An} = \frac{\text{Annual power output (electrical power)}}{\text{Annual power input (spectral power)}} = \frac{\sum_{a=1.0}^{11.5} f(a)P_{sc}(a)\Delta a}{\sum_{a=1.0}^{11.5} f(a)P_{sun}(a)\Delta a} \quad (5)$$

where $P_{sc}(a)$ and $P_{sun}(a)$ are the electrical power output of the solar cell (calculated as described above) and the spectral power input respectively for AM a. The seasonal calculations involve similar summations, using the relevant $f(a)$ values. The results of these calculations depend on the values chosen for parameters input to SPCTRAL2 at each AM interval and on the solar radiation component (direct or global).

Figures 4(a) and 4(b) show the effect of latitude on summer (June 21 to September 21) and winter (December 21 to March 21) partition of energy with AM ($f(a)P_{sun}(a)$), as defined above. With increasing latitude, the energy partition shifts towards the higher AM. The effect of latitude on energy distribution is greater for winter than summer, *i.e.* there is a larger shift towards higher AM and greater attenuation of energy. Summer partition of the energy by AM is nearly constant for a wide range of latitudes.

The annual distribution of energy by AM value for the global-normal case is shown in Fig. 4(c). For higher latitudes two maxima appear that correspond to days around June 21 and December 21. A similar result was

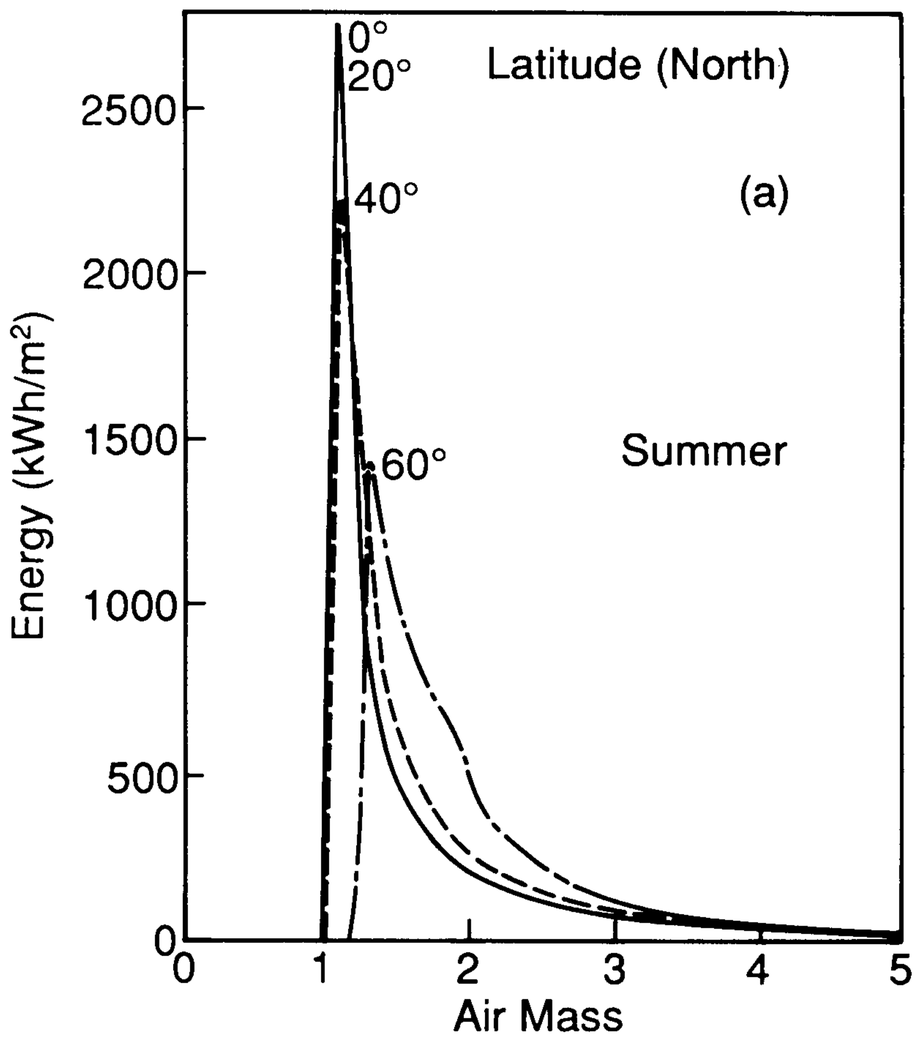

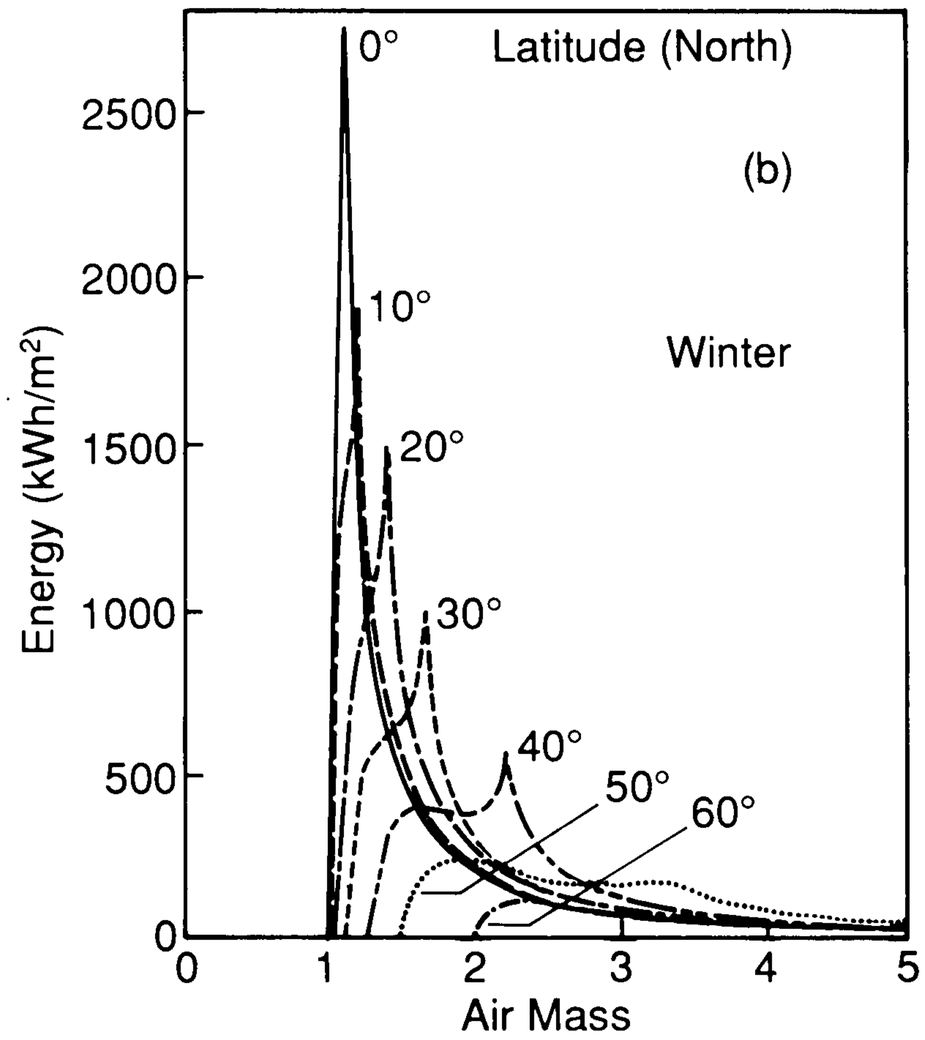

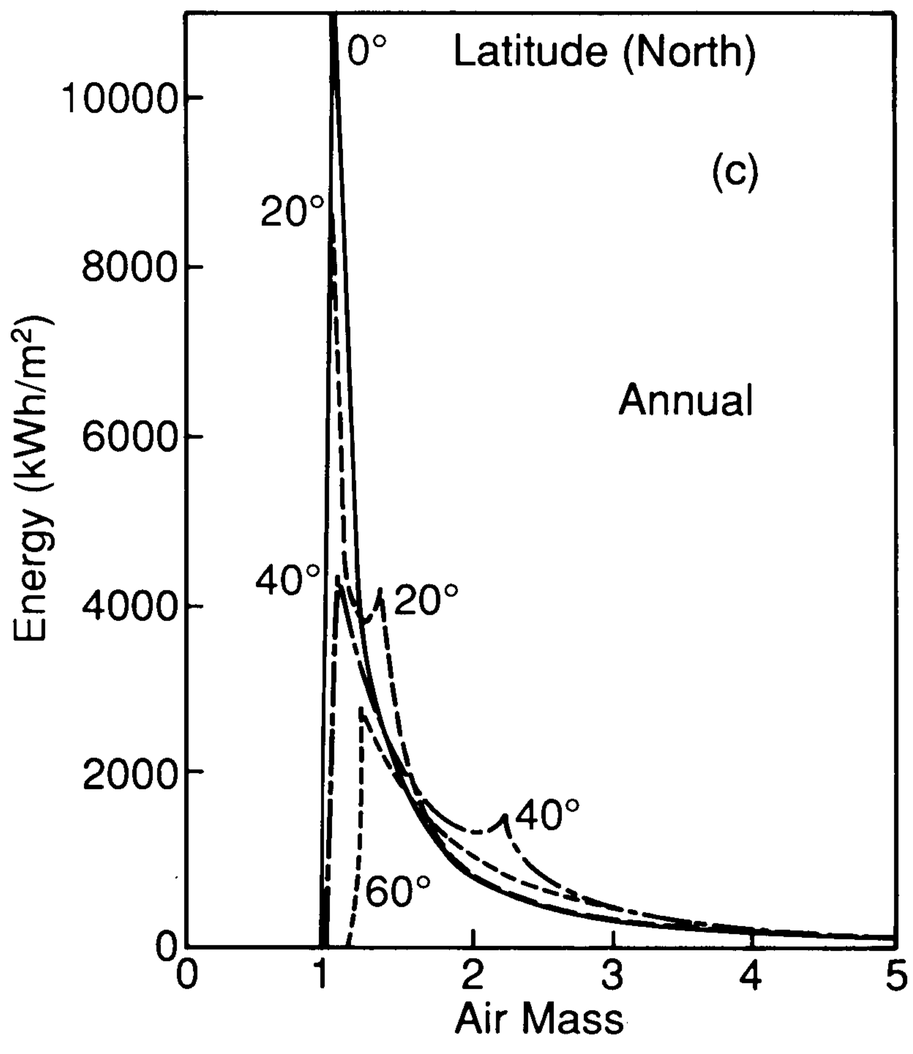

Fig. 4. Distribution of the summer (June 21 to September 21) (a), winter (December 21 to March 21) (b) and total annual (c) solar energy as a function of air mass for latitudes between 0° and 60°. The shapes of the curves are fairly independent of spectrum, but the absolute energy scales assume a global-normal spectrum with a water vapor of 1 cm, turbidity of 0.2 at sea-level and no clouds.

obtained for the direct-normal case; however, the total energy was about 20% lower because of the absence of the diffuse component.

3. Results

3.1. Instantaneous effects of spectral parameters

3.1.1. Sensitivity of solar cell performance to AM variations

As the solar zenith angle varies with time or latitude, the AM variations

affect the distribution and magnitude of photon density in the spectrum (see Fig. 1). Higher AMs result in a shift of the photon distribution towards longer wavelengths, or lower energies, so that the effect on solar cells is dependent on bandgap, with high-bandgap cells being most strongly affected. AM effects are slightly larger for direct than for global spectra because some of the photons that are scattered out of the direct beam are added back as the diffuse component of global spectra.

Figure 5 shows how AM variations affect solar cell performance. For MJ-2T solar cells, the LE_g combination is less sensitive to AM than the HE_g combination. The current mismatch due to AM in the HE_g combination is important for higher AMs because the high-energy region of the photon distribution becomes strongly unbalanced between the UV–visible (below 0.78 μm) and near-IR (NIR, above 0.75 μm) regions. Because the 2J-2T-LE_g cell collects photons over a range of energies which is twice as large, the photon distribution is not as critical.

The efficiency of the 2J-4T-LE_g cell degrades with AM at about the same rate as the 1J-HE_g cell because in both cases the degradation is determined by a GaAs cell. However, the 2J-4T-HE_g cell is affected more than the 1J-HE_g cell. Therefore MJ-HE_g cells are the most sensitive to AM variations, even when designed as 4T devices. Large current mismatches in the 2T configuration increase their sensitivity at high AM. The impact of this sensitivity on average cell performance is discussed later.

3.1.2. Sensitivity of solar cell performance to turbidity

Increased turbidity causes more attenuation and scattering of solar irradiance in the UV–visible compared with the NIR region of the spectrum. Therefore HE_g cells are affected more than LE_g cells as shown in Fig. 6. For comparison, the decrease in spectral power is also shown in Fig. 6.

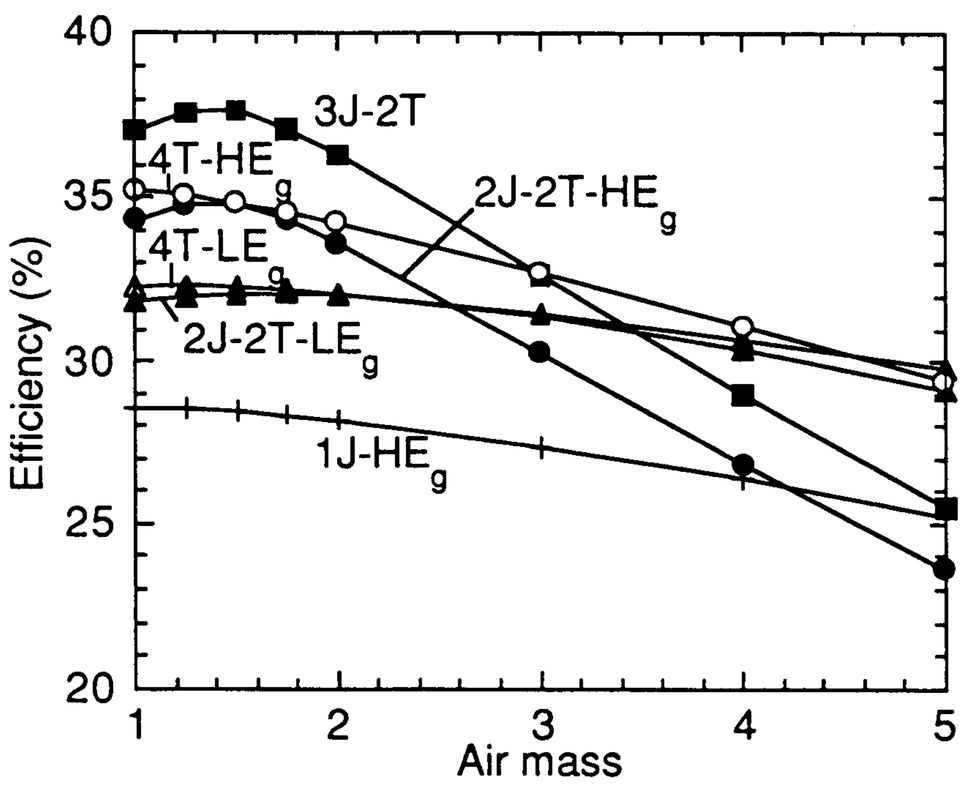

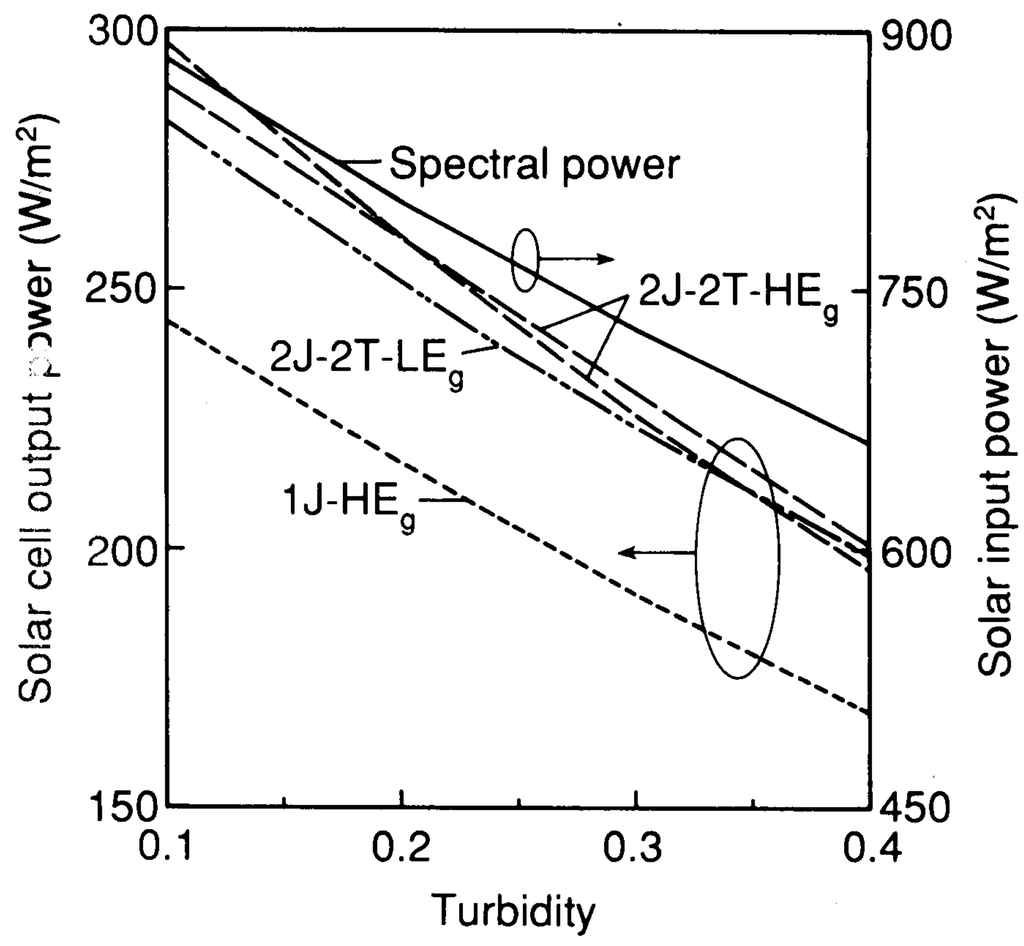

Fig. 5. Efficiencies of six different cell designs as a function of air mass for global-normal one-sun spectra at 1580 m, water vapor of 1 cm and turbidity of 0.2.

Fig. 6. Power output fo' ne single-junction and three (two-terminal) multijunction cells as a function of turbidity for direct-normal one-sun spectra at AM 1.5 and a water vapor of 1 cm.

Because some of the scattered photons are collected when the global component of the irradiance is considered, the effect of turbidity is larger for cells under direct-normal than under global-normal irradiance (not shown). Combined with AM variations, turbidity can result in a high current mismatch for MJ-2T-HE_g cells. In Fig. 6 the two curves labeled 2T-HE_g have slightly different top-cell thicknesses, and thus demonstrate the effect of the current mismatch. The dominant factor in the reduced power output for all the cells is the lower spectral power for high turbidity, but the 2J-2T-HE_g cell degrades faster than the 2J-2T-LE_g cell as the turbidity is increased.

3.1.3. Sensitivity of solar cell performance to water-vapor variations

The power output of LE_g devices is expected to be more sensitive to water-vapor variations than the HE_g devices because of the overlap of the spectral response with the water absorption bands in the spectrum (see Fig. 3). When the spectral response of a solar cell overlaps a water-vapor absorption band, both the output power of the cell (numerator in efficiency calculations) and the total irradiance (denominator) are reduced. Otherwise, only the denominator is reduced which results in a higher calculated efficiency, even though the power output of the cell is not affected.

For SJ cells with an E_g equal to or higher than 1.4 eV, there is a 1%–2% decrease in power output, as water vapor varies from 1 to 5 cm. The spectral power decreases by 6%–7% for the same change of water-vapor parameter. For LE_g cells such as silicon or germanium, up to a 10% decrease in power output is observed. If only the direct-normal spectrum is considered, the water-vapor effect is slightly higher for LE_g devices because a higher percentage of photons are in the NIR region as compared with the global-normal case. MJ-LE_g cells are also affected more by water vapor than MJ-HE_g cells.

Figure 7 shows the current mismatch due to water-vapor absorption for both kinds of MJ-2T cell. The short-circuit currents for the 2J-2T-LE_g and 2J-2T-HE_g devices with a water vapor of 1 cm are 24.5 and 13.5 mA cm^{-2} respectively. The 2J-2T-LE_g cells are more sensitive because the higher absorption in the low-energy region results in a large current mismatch. Because of the location of the important water-vapor absorption bands, the bottom-cell current of an LE_g cell is strongly affected, whereas the top-cell current is only slightly affected. If the 2J-2T-LE_g cell was designed for a mid-range water-vapor amount (*e.g.* 3 cm) rather than a low water-vapor amount, the maximum current mismatch would be reduced for cases when the solar cell is operated outdoors in a range of low to high water-vapor conditions. However, because of a large increase in fill factor (see discussion below), the current mismatch shown in Fig. 7 is much greater than the loss in efficiency.

The water-vapor effect is less important than the turbidity effect. Turbidity acts more like a broad-band filter with a higher attenuation for higher energies. Water vapor affects specific wavelength bands and, therefore, only particular types of device which overlap these absorption bands.

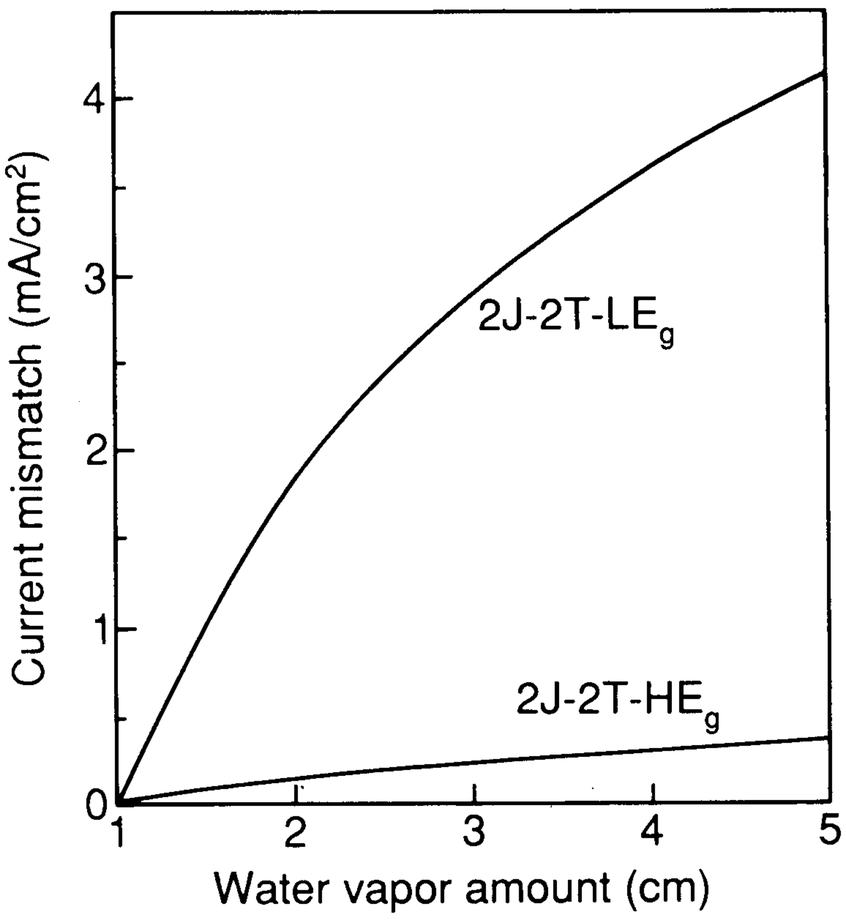

Fig. 7. Current mismatch in the high- and low-bandgap two-terminal multijunction cells as a function of water-vapor amount for direct-normal one-sun spectra at AM 1.5, sea-level and a turbidity value of 0.1. The thicknesses of the top cells were optimized for a water vapor of 1 cm. The bandgap of the lower cell for the 2T-LE_g cell was set to 0.8 eV.

3.2. Average power output of MJ and SJ cells

The average power output of solar cells is a function of spectral parameters as shown above. The water-vapor content and turbidity vary in a complex and unpredictable way from place to place and time to time. However, the variation of AM is a predictable function of location (latitude) and time (both time of day and day of the year). In this section we discuss the variation of power output for various times of the day and year assuming cloudless skies, and integrate the relative power outputs in order to compare the seasonal or annual energy output for the different cell designs.

3.2.1. Daily variations of power output

Figure 8 shows the AM variations on three specific days of the year (solstices and equinox) and latitude 40 °N. The power outputs of the different types of cell are plotted *vs.* hour of the day in Fig. 9 based on the summer and winter AM variations shown in Fig. 8. The large difference in the performance during winter and summer is due to differences in day length and AM. The integrated energy output over the day and the corresponding average efficiency of each device for these two days and for September 21 are shown in Table 2. For comparison, the predicted efficiencies using the AM 1.5 design spectrum described above are also given in Table 2. Table 3 gives similar information for cells designed and averaged under global-normal conditions. As can be seen from Tables 2 and 3, there is little difference between the effects of AM under global-normal and direct-normal conditions.

Although HE_g cells are very sensitive to AM variations (*e.g.* decrease of more than 10% absolute efficiency as AM is increased from 1 to 5, see Section 2), it can be seen from Tables 2 and 3 that the average efficiency calculated from the integrated power is almost as high as the AM 1.5 values.

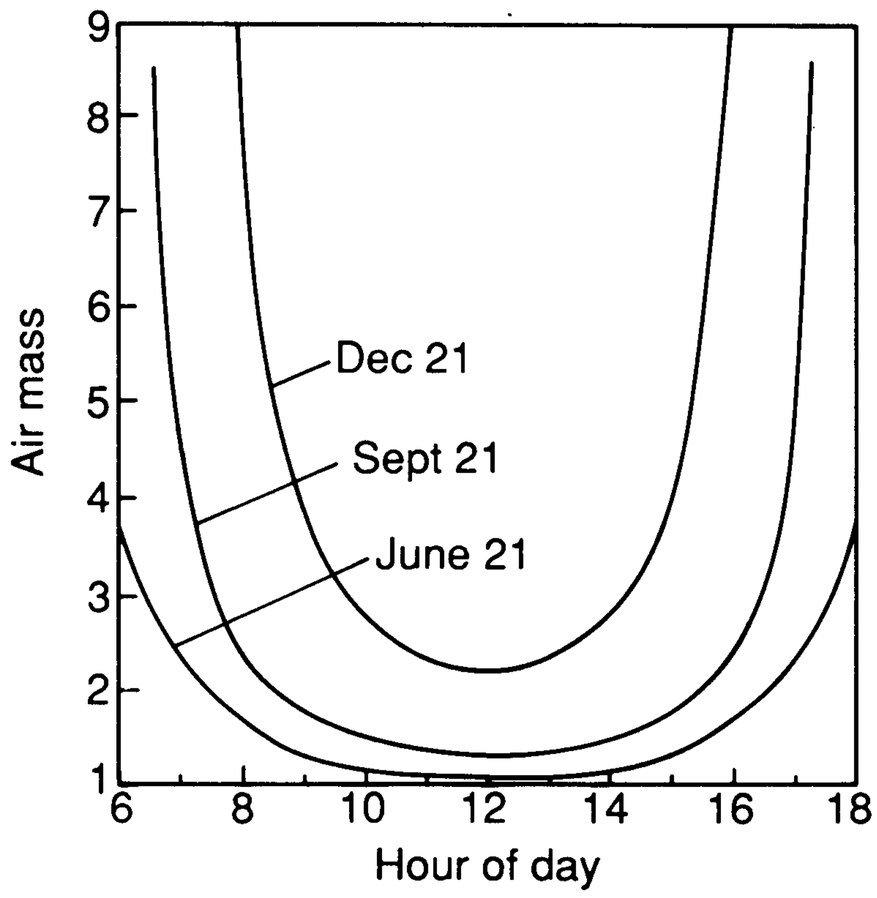

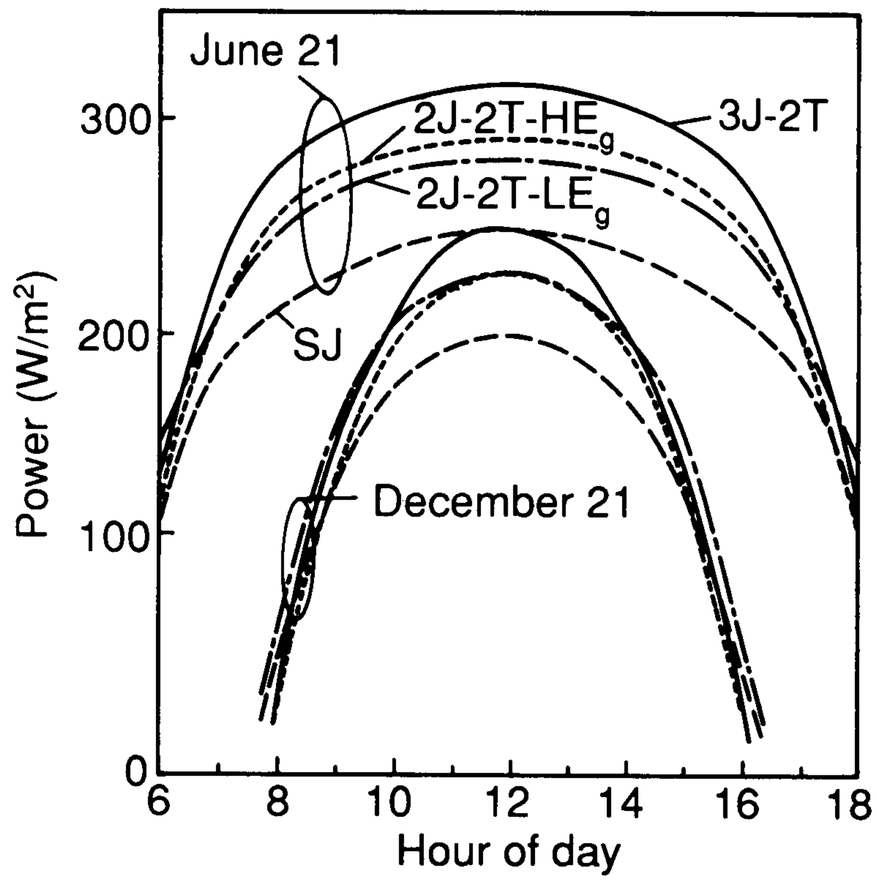

Fig. 8. Air mass variation with hour of the day for three different days of the year in Golden, CO (latitude approximately 40 °N).

Fig. 9. Power output of four different types of two-terminal cell as a function of the hour of the day for summer and winter direct-normal one-sun conditions at Golden, CO (see Fig. 8).

Figure 8 shows that high AM conditions at latitude 40 °N occur for a short time during the day. In addition, the total solar intensity is relatively low at the higher AMs, so that the efficiency of a device at high AM makes little difference in the daily output. This observation has also been made by others [13–15].

The only devices that show much sensitivity are the 2J-2T-HE_g and 3J-2T cells. As shown in Tables 2 and 3, the performance of the 2J-2T-HE_g cell decreases in winter much more than that of the 2J-2T-LE_g cell. The increased AMs in winter lead to higher current mismatches for this cell than for any of the other cells studied. Therefore its performance is expected to degrade during winter, especially at high latitudes. As shown in Fig. 9, the 2J-2T-LE_g cell has a stable performance through the seasons which is comparable with that of the single-junction GaAs cell, because they are both less sensitive to AM variations (see Fig. 5).

The power output through the day for 4T and 2T cells is plotted in Fig. 10. The difference in power output between the 2T and 4T configurations gives the loss in power due to current mismatch. The 2J-2T cells are current matched for AM 1.5 conditions, which occur at hours 8 (a.m.) and 16 (p.m.) on June 21 (see Fig. 8). In winter, AM is always larger than 1.5 at this latitude; therefore the 2T cell currents are never matched. The 2J-2T-LE_g cell mismatch losses are lower than 1% at the maximum and are as low in winter as in summer. The mismatch losses in the 2J-2T-HE_g cells are higher.

A closer look at what happens when the currents become mismatched shows that both the current and fill factor change. The open-circuit voltage is fairly insensitive to current mismatch because it is mostly a function of E_g. However, an increase in current mismatch is partly compensated by an increase in fill factor as shown in Fig. 11. When the current mismatch is 10% of the short-circuit current, the fill factor increases by 2% and 5% for

TABLE 2

Energy output and average efficiency of two-terminal devices under cloudless direct-normal irradiance spectra at 40 °N latitude

Device	AM 1.5 (%)	June 21		September 21		December 21		Annual
		Output (kWh m^{-2})	Efficiency (%)	Output (kWh m^{-2})	Efficiency (%)	Output (kWh m^{-2})	Efficiency (%)	Efficiency (%)
1J-HE_g	27.1	2.75	26.7	2.1	26.5	1.23	25.4	26.4
2J-2T-HE_g[a]	32.8	3.22	31.3	2.5	31.1	1.35	27.8	30.7
2J-2T-LE_g[a]	31.4	3.19	31.0	2.5	30.9	1.45	29.8	30.2
3J-2T[a]	35.3	3.46	33.6	2.7	33.4	1.46	30.1	33.0

[a]Top cell optimized for direct-normal AM 1.5 spectrum at one sun with turbidity of 0.2 and water-vapor amount of 1 cm.

TABLE 3

Energy output and average efficiency of two-terminal devices under cloudless global-normal irradiance spectra at 40 °N latitude

Device	AM 1.5 (%)	June 21		September 21		December 21		Annual
		Output (kWh m^{-2})	Efficiency (%)	Output (kWh m^{-2})	Efficiency (%)	Output (kWh m^{-2})	Efficiency (%)	Efficiency (%)
1J-HE_g	28.5	3.52	28.0	2.79	27.9	1.68	27.1	27.9
2J-2T-HE_g[a]	34.8	4.17	33.1	3.29	32.9	1.84	29.7	32.5
2J-2T-LE_g[a]	32.1	3.97	31.5	3.16	31.6	1.92	31.0	31.6
3J-2T[a]	37.6	4.50	35.7	3.56	35.6	1.99	32.1	35.1

[a]Top cell optimized for global-normal AM 1.5 spectrum at one sun with turbidity of 0.2 and water-vapor amount of 1 cm.

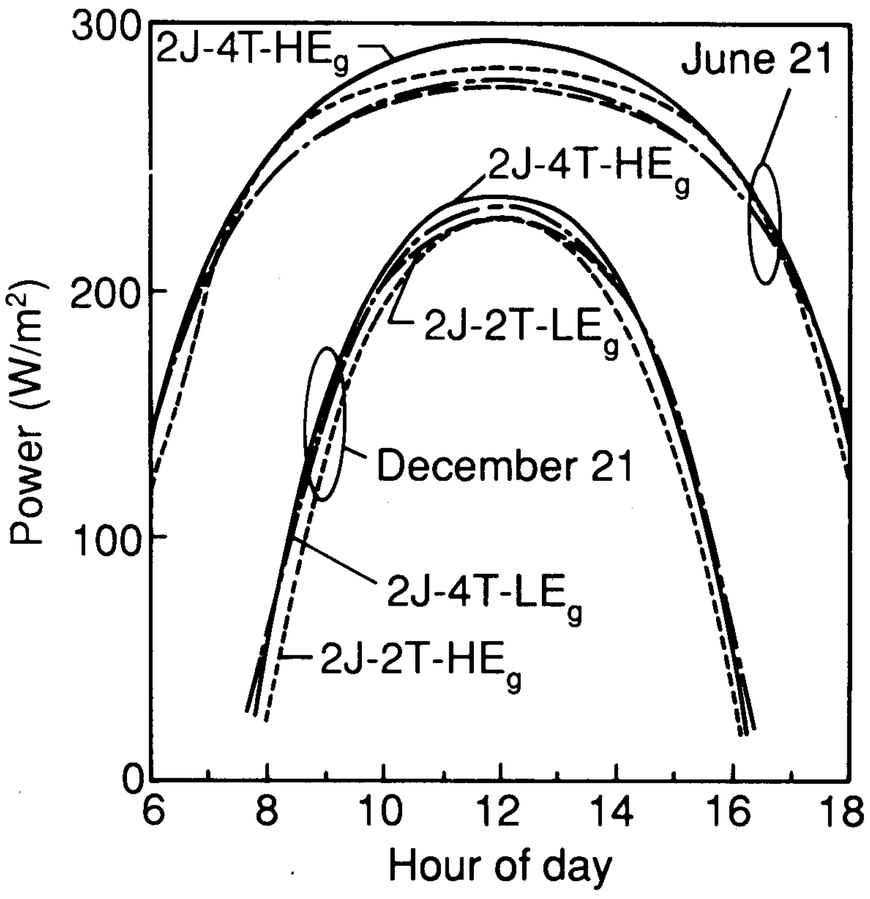

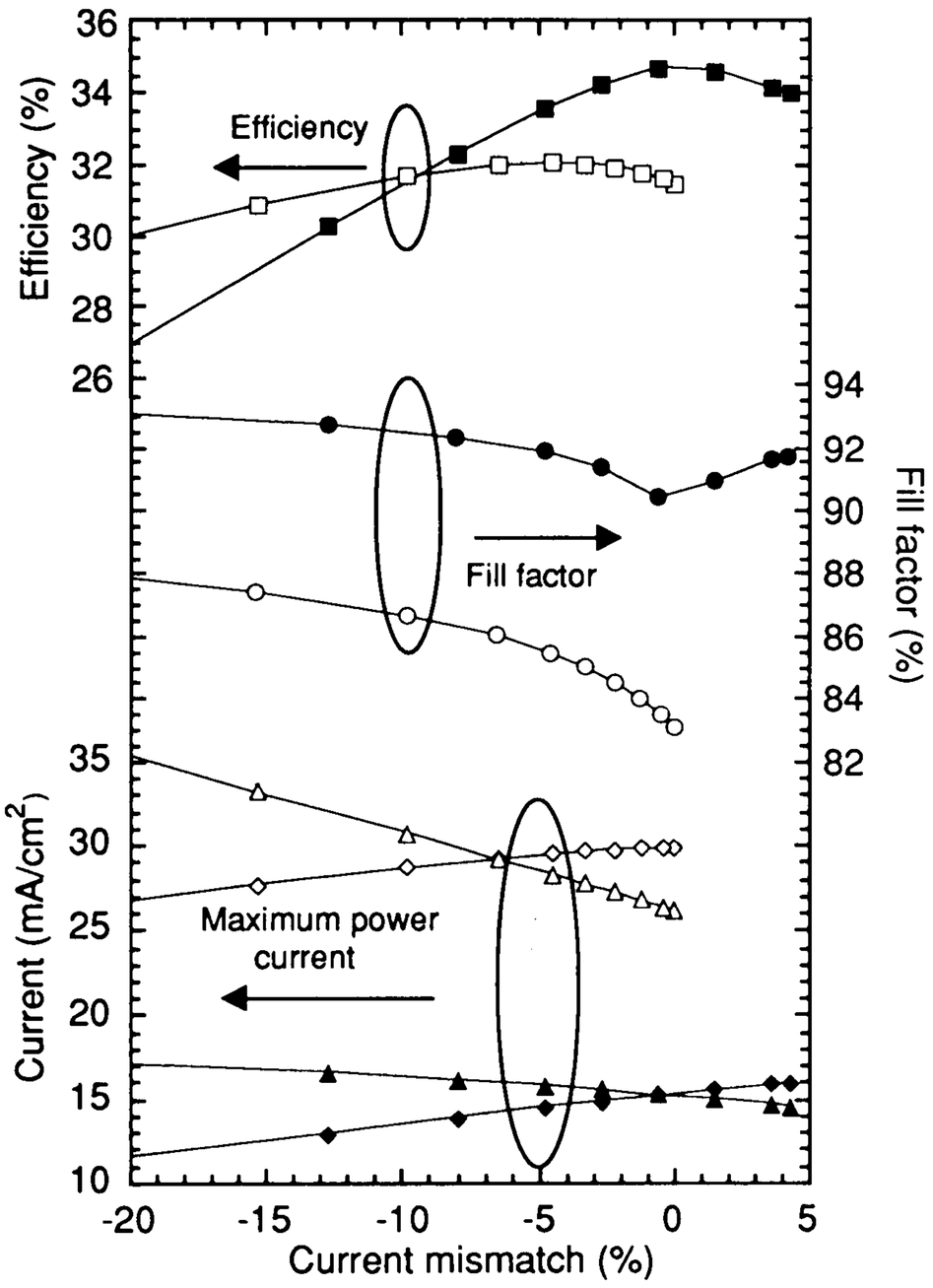

Fig. 10. Comparison of the power outputs of two-terminal and four-terminal multijunction cells as a function of the hour of the day for summer and winter days using direct-normal one-sun spectra at Golden, CO (see Figs. 8 and 9).

Fig. 11. Efficiency, fill factor and top- and bottom-cell currents at the maximum-power point as a function of the short-circuit current mismatch for 2J-2T-HE_g (filled symbols) and 2J-2T-LE_g (open symbols) cells. The current mismatch plotted on the x axis is calculated from $(J_{\mathrm{Ltop}} - J_{\mathrm{Lbottom}})/(J_{\mathrm{Ltop}} + J_{\mathrm{Lbottom}})$. The variable mismatch is a result of varying air masses such as those demonstrated in Figs. 8–10. However, the data shown in this figure were calculated for a constant irradiance (*i.e.* the concentration was adjusted for each air mass).

the HE_g and LE_g cells respectively. Thus the actual decrease in efficiency is substantially less than would be predicted from a study of short-circuit currents alone. The increase in the fill factor as the current mismatch increases has been experimentally measured outdoors by Morel *et al.* [16] for Si/Ge MJ-2T cells. Clearly, this effect is most beneficial for LE_g or other cells with smaller fill factors. However, we should also note that the LE_g cells are more difficult to current match because a 2J-2T-LE_g cell that is current matched under the short-circuit current condition is not matched at the maximum-power point (*i.e.* the point in Fig. 11 where the top- and bottom-cell currents cross.) The fill factor is smallest for both LE_g and HE_g cells when they are current matched at the short-circuit condition, and the efficiency is maximized when they are matched for the maximum-power point. In general, the efficiency of the LE_g cells is less sensitive to current mismatch because the fill factor can increase significantly to compensate partially for the mismatch.

Similar to their consistent performance with the AM fluctuations encountered during one day, LE_g cells are slightly more stable in performance through the seasons as shown in Fig. 12. Here, the power outputs of the different cells have been calculated for each day of the year. Going from

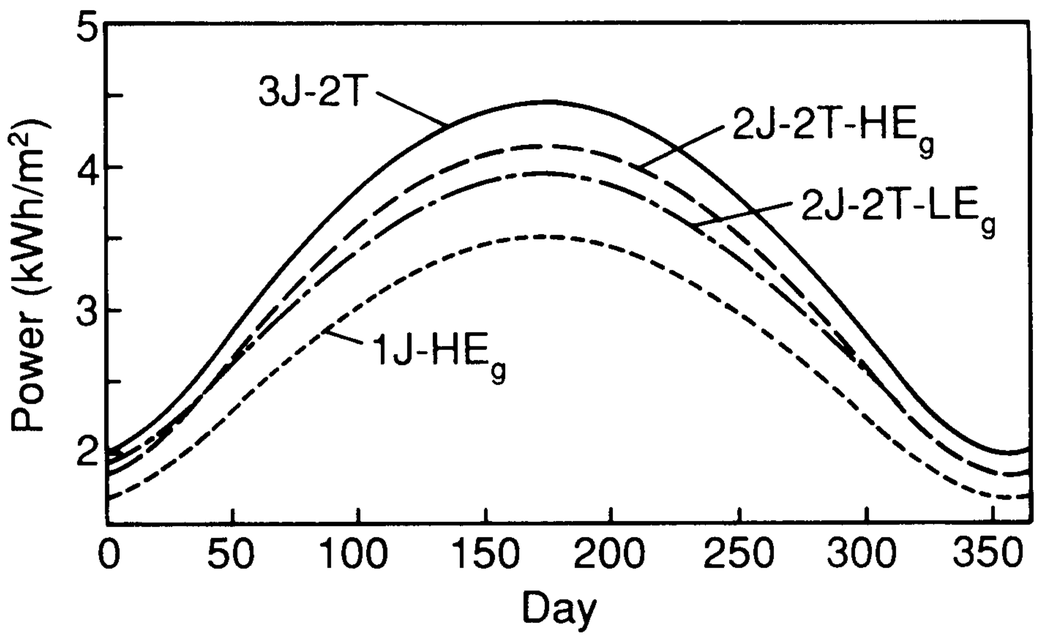

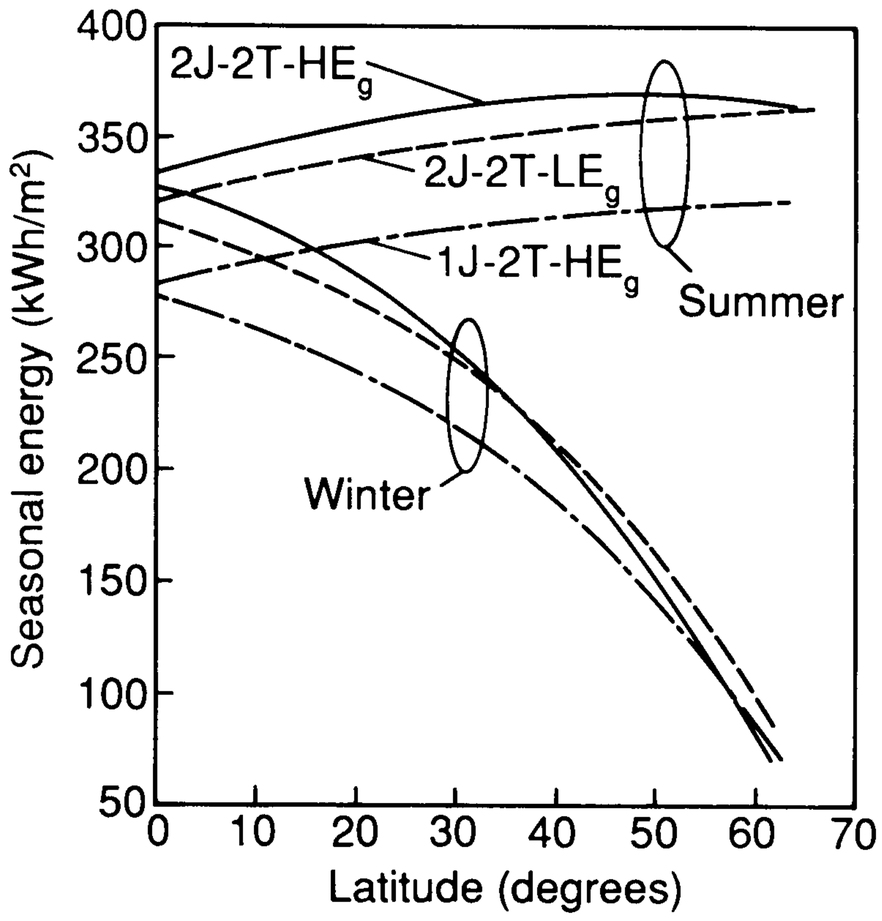

Fig. 12. Power output of four different cells as a function of the day of the year for global-normal one-sun spectra at Golden, CO (latitude approximately 40 °N) (water vapor, 1 cm; turbidity, 0.2).

Fig. 13. Summer (June 21 to September 21) and winter (December 21 to March 21) integrated power outputs of three different cells as a function of latitude for global-normal one-sun spectra at sea-level (water vapor, 1 cm; turbidity, 0.2).

one to two junctions allows a gain in power of 18% in summer and 10% in winter for the 2J-2T-HE_g cell, and 12% in summer and 15% in winter for the 2J-2T-LE_g cell.

3.2.2. Integrated annual and seasonal power output

Seasonal performance is a strong function of latitude because the AM distribution functions shown in Fig. 4 depend on latitude. As long as this distribution varies slowly with latitude (for low latitudes), device performance is expected to be constant. For higher latitudes, the AM density function varies rapidly with latitude. Therefore the device performance is constant over a narrower range of latitude, especially if the device is sensitive to AM variations.

Figure 13 shows how HE_g devices are more sensitive to latitude than LE_g devices during the winter months. Higher AMs at high latitudes affect the current matching in the 2J-2T-HE_g and 3J-2T cells. The difference in performance between winter and summer increases with latitude, and device performance is affected most during the winter. The 2J-2T-HE_g cell performance becomes comparable with the 1J-HE_g cell performance in winter when the latitude is high. The increase in performance in summer for each type of cell is due to the increasing day length in summer with latitude.

The annual power outputs for the six different cell structures are shown in Fig. 14 as a function of latitude. The energy outputs of all the cells are strongly dependent on latitude for latitudes greater that 30°. Because the 2J-2T-HE_g and 3J-2T cells are more sensitive to high AM, and therefore to winter variations, their annual performance decreases faster with latitude compared with the other devices.

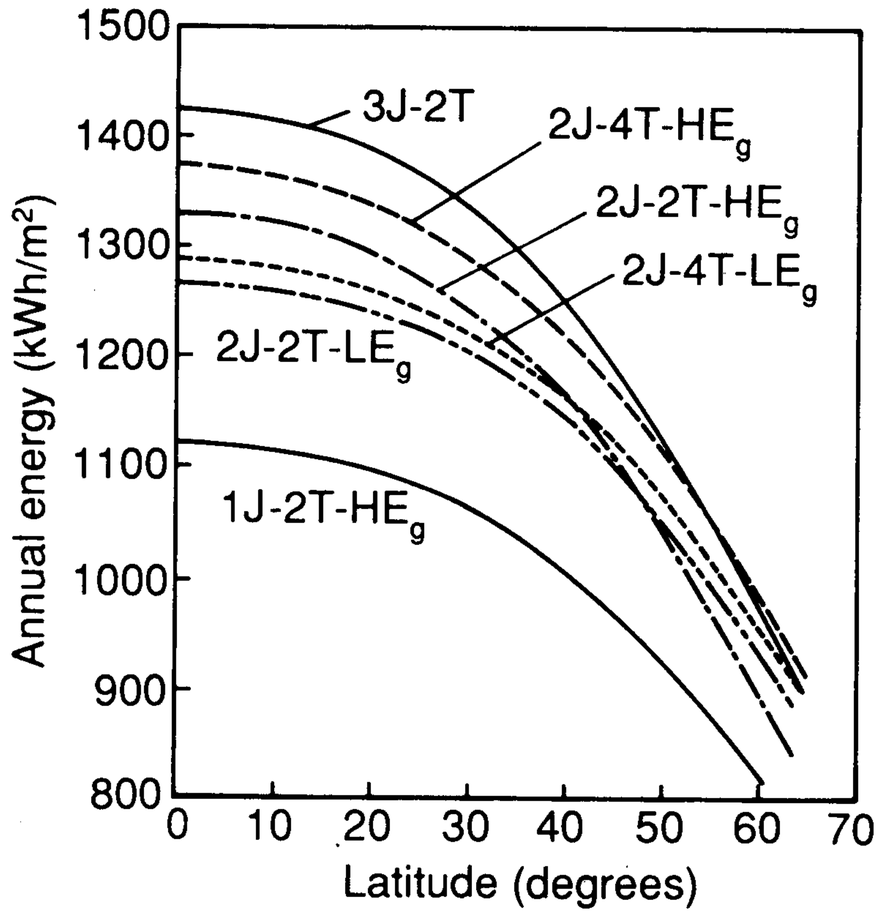

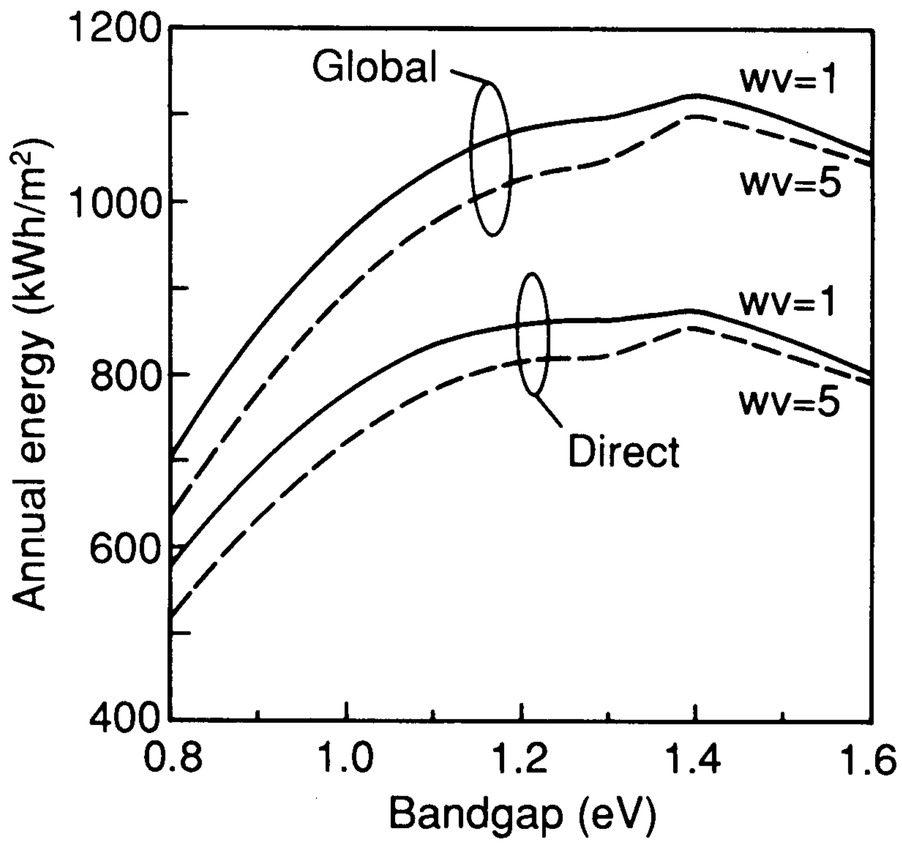

Fig. 14. Effect of latitude on the integrated annual power output for various cell designs for global-normal one-sun spectra at sea-level (water vapor, 1 cm; turbidity, 0.2).

Fig. 15. Annual performance of single-junction cells as a function of bandgap and amount of water vapor (latitude, 0°; sea-level; turbidity, 0.2; no clouds).

Annual losses resulting from current mismatch are given by the difference in performance between the 2T and 4T configurations. A constant loss of 1.5%–2% of the annual energy output is a result of mismatch in the 2J-2T-LE_g device. This is similar to the results of King and Siegel [17], who calculated that the penalty in performance resulting from series connection relative to independent connection was less than 2% over the year for an optimized Si/AlGaAs MJ cell in Albuquerque, NM (about 35° N latitude). For 2J-2T-HE_g cells, the annual energy loss resulting from current mismatch is 3.3% at the equator, 3.4% at 20° of latitude, 4.8% at 40° and 8.3% at 60°.

The annual sensitivity of the SJ cells to water-vapor variations is shown in Fig. 15. Water vapor affects the performance of LE_g cells the most because water absorption bands are located mostly at longer wavelengths. The performance of SJ-HE_g cells decreases by only 2%, but the performance of SJ-LE_g cells decreases by up to 10%. This calculation shows only extreme cases, as it assumes that the climate is fairly dry or humid all year long. King and Siegel [17] performed a more realistic simulation in which the water-vapor amounts were varied throughout the year.

The dependence of the performance of MJ-2T devices on water vapor can also be estimated from Fig. 15. If the bandgaps are chosen to be higher than 1.4 eV, the current mismatch will be small. However, if one of the bandgaps is low (such as 0.6–1.1 eV), the bottom-cell current will be decreased by up to 10%, whereas the top-cell current is decreased by only 2%. Therefore current mismatch may limit 2J-2T-LE_g cell performance in a humid climate. Annual direct-normal performance calculations for MJ devices in dry and humid climates show that the 2J-2T-HE_g cell performance decreases by 1.8%, whereas the 2J-2T-LE_g cell performance decreases by 6.2%, for the same change in water-vapor amount as shown in Fig. 15, using a latitude of 40 °N.

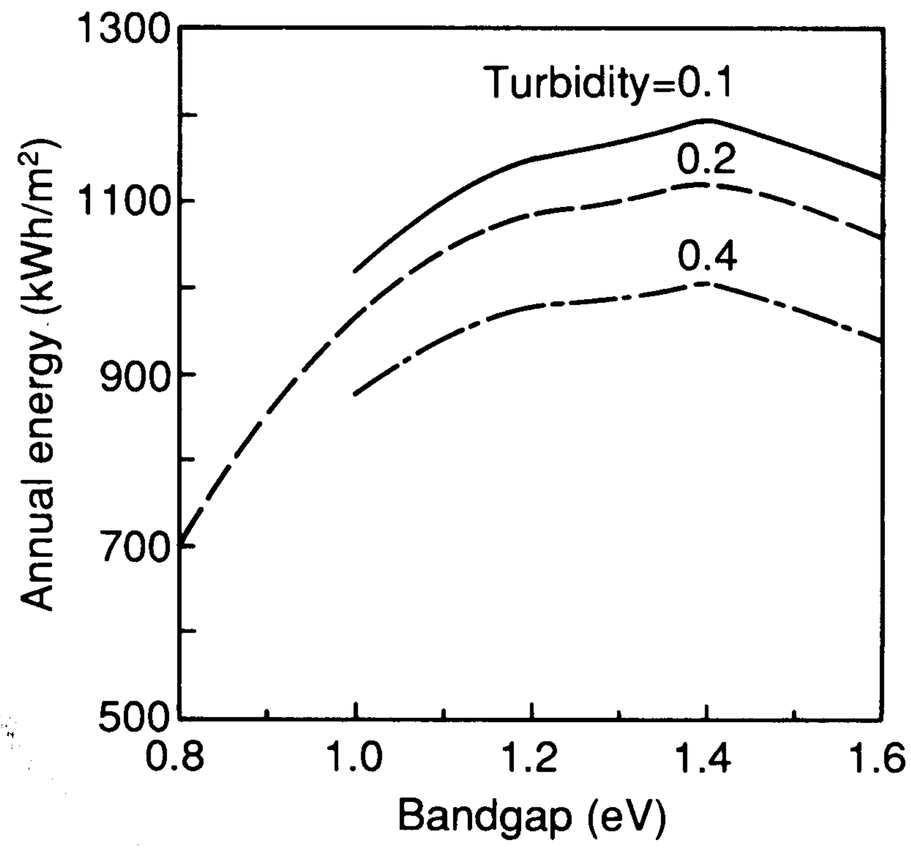

Fig. 16. Annual performance of single-junction cells as a function of bandgap and turbidity (global-normal one-sun spectra; latitude, 0°; sea-level; water vapor, 1 cm; no clouds).

Turbidity has a much greater effect on solar cells than does water vapor as shown in Fig. 16. Up to 20% of the energy output is lost for HE_g cells, although most of this decreased power output is because of decreased spectral power. The decrease is slightly lower for LE_g cells. The current mismatch of 2J-2T-LE_g cells resulting from turbidity is small. Because the attenuation resulting from turbidity is higher for higher energies, the current mismatch of 2J-2T-HE_g cells is more important. In all cases, the attenuation resulting from high turbidity drastically limits the performance of all solar devices.

The 2J-4T cells are affected almost as much as 2J-2T cells by turbidity because turbidity acts more like a broad-band filter than does water vapor. A small gain can be expected in the 4T configuration compared with the 2J-2T-HE_g configuration. The 2J-4T-LE_g cell out-performs the 2T configuration when water vapor varies, because current mismatch limits the 2T cell performance. However, the gain is only a few percentage points (relative). The 2J-2T-HE_g cell is almost as insensitive to water vapor as the 4T cell because no current mismatch is observed.

3.3. Effect of latitude on device design

Although solar cells are often designed for optimum performance at standard ASTM AM 1.5 spectral conditions, it is important to realize that the ASTM spectra are more appropriately used for comparing the performance of solar cells under those particular spectral irradiance conditions. Because spectral irradiance depends on atmospheric and AM conditions, the AM 1.5 standard spectra do not necessarily represent average or typical spectral conditions at an arbitrary location. (However, in generating the spectral irradiance data sets that were subsequently adopted as standard spectra by ASTM, an attempt was made to select representative atmospheric and AM conditions for the United States [3].) As pointed out by Riordan and Hulstrom [4] and others [16], a specific AM spectrum is not necessarily ideal for optimizing energy output at an arbitrary location.

We investigate here the advantage of designing a PV device for optimal outdoor performance at a particular location. We have shown that the latitude has an important influence on cell performance at a particular location. For low latitudes the solar zenith angle is low most of the time, and the AM is therefore low. For high latitudes the solar zenith angle is high and the AM high. Because MJ-HE_g cells show greater sensitivity to AM fluctuations, MJ cells could be designed so that their performance would be optimal most of the time. Ideally, the cell is optimized by multiplying the AM density function (Fig. 2) with the device efficiency (Fig. 3) and integrating over AM for a number of device designs. However, this is a laborious procedure, and a quick estimate can be obtained by assuming that the variations in the strongly peaked AM density function (Fig. 2) are much more important than the variation in the device efficiency as a function of AM (Fig. 3). With this assumption, the cells should be designed for optimum results at the average AM condition. This particular value of AM is a function of latitude because larger zenith angles result from higher latitudes.

To calculate the average AM condition at a specific latitude, we used the data shown in Fig. 4 and calculated the AM value for which the integrated energy from AM 1 to this value was half of the total integrated energy from AM 1 to AM∞. This calculation was performed for summer, winter and annual AM distributions, and the result is shown in Fig. 17. Both global-normal and direct-normal components result in the same set of curves.

The annual curve is intended to be used for optimizing the annual energy output. The winter curve can help to design MJ cells when high energy output is required in winter. If energy output is only important during summer, a single design of MJ cell (for AM 1.25–1.3) is optimum for a wide range of latitudes.

We calculated the annual energy output of the 2J-2T-HE_g cell designed for three different latitudes (0°, 40° and 60°) according to Fig. 17. The top-cell thicknesses were adjusted for current matching at the appropriate AM for each latitude. The annual performance of each cell was calculated for the three latitudes and global-normal irradiance, and the results are shown in Table 4. As expected, at each particular latitude, the cell that out-performs

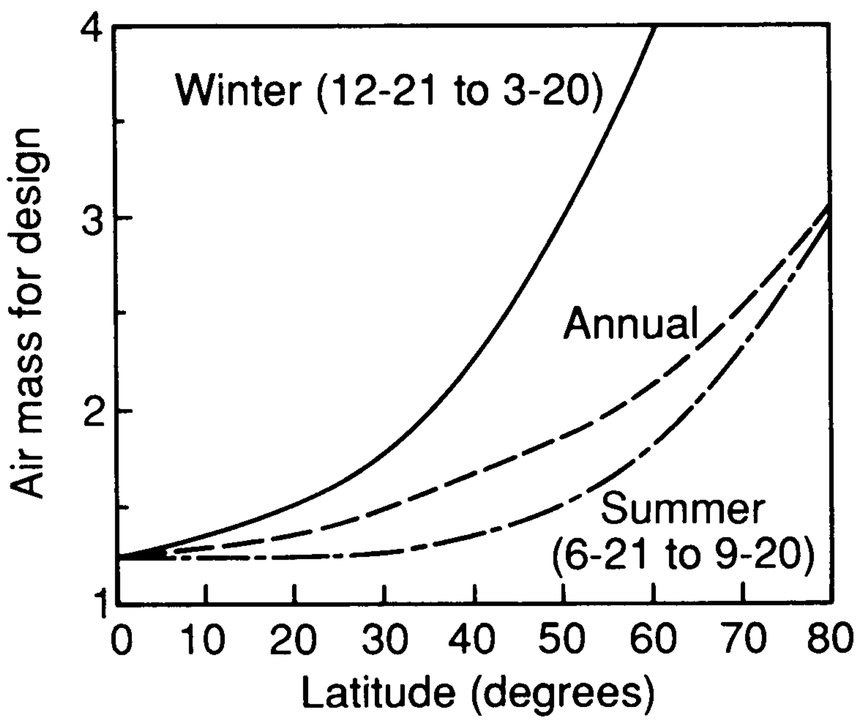

Fig. 17. Optimal AM for design of cells as a function of latitude (sea-level; water vapor, 1 cm; turbidity, 0.2; no clouds).

TABLE 4

Relative annual (cloudless-sky) performance of 2J-2T-HE_g cells using latitude as a design parameter

Device optimized for	Annual performance (kWh m^{-2})		
	0°	40 °N	60 °N
AM 1.25 (0° latitude)	1328	1162	895
AM 1.7 (40° N latitude)	1317	1173	916
AM 2.1 (60 °N latitude)	1291	1164	919

the others is the one designed for that specific latitude. However, the gain in performance attributable to latitude design is small (less than 3%). Moreover, the cell that leads to the best average performance over this range of latitudes is the one designed for mid-latitude (40°). Therefore use of the standard AM 1.5 is adequate to account for AM variations for latitudes less than 60°. However, as shown elsewhere [7], when coupled with other variations in parameters (turbidity and surface pressure), redesigning the cell for each site may yield substantial improvement in the average performance. Because variations in manufacturing conditions could result in a variety of cells, it is unclear whether this is an advantage or disadvantage.

4. Conclusions

The effects of variations in solar spectral irradiance depend on the bandgap of the device as well as on the number of junctions. Turbidity and air mass fluctuations affect the performances of high-bandgap devices more than those of low-bandgap devices. However, water-vapor fluctuations have very little effect on high-bandgap devices compared with low-bandgap devices.

Air mass fluctuations during a year are important for series-connected high-bandgap devices. However, the loss of performance is not as extreme as would be predicted from current mismatch as a function of air mass. This is true because little power is delivered at high air mass and because an increase in fill factor somewhat offsets the current mismatch. The effects of spectral fluctuations are significant and should be considered when predicting outdoor performance of devices. However, the variations in cell performance are sufficiently small to be given only secondary consideration, with primary consideration given to the absolute performance. Thus if the theoretical efficiencies can be achieved, multijunction cells are expected to out-perform single-junction cells even after spectral fluctuations are considered. Although the average performance increases slightly, there is little advantage in designing a multijunction cell for optimal performance at the latitude for which it is intended.

References

1 American Society for Testing and Materials (ASTM), *Standard Tables for Terrestrial Direct Normal Solar Spectral Irradiance for Air Mass 1.5, E891-87*, ASTM, Philadelphia, PA.

2 American Society for Testing and Materials (ASTM), *Standard Tables for Terrestrial Solar Spectral Irradiance at Air Mass 1.5 for a 37° Tilted Surface, E892-87*, ASTM, Philadelphia, PA.

3 R. Hulstrom, R. Bird and C. Riordan, *Sol. Cells, 15* (1985) 365–391.

4 C. Riordan and R. Hulstrom, Summary of studies that examine the effects of spectral solar radiation variations on PV device design and performance, *SERI/TR-215-3437*, Solar Energy Research Institute, Golden, CO, March, 1989.

5 R. Bird and C. Riordan, *J. Climate Appl. Meteorol., 25* (1986) 87–97.

6 S. Kurtz, P. Faine and J. Olson, *J. Appl. Phys., 68* (1990) 1890.

7 S. Kurtz, J. Olson and P. Faine, *Sol. Cells*, in the press.

8 S. Nann and C. Riordan, *Proc. 21st IEEE Photovoltaic Specialists Conf., Kissimmee, FL, 1990*, IEEE, New York, 1990, p. 1110.

9 S. Nann and C. Riordan, *J. Appl. Meteorol., 30* (1991) 447–462.

10 J. C. C. Fan, B.-Y. Tsaur and B. J. Palm, *Proc. 16th IEEE Photovoltaic Specialists Conf., San Diego, CA, 1982*, IEEE, New York, 1982, p. 692.

11 M. E. Nell and A. M. Barnett, *IEEE Trans. Electron Devices, 34* (1987) 257.

12 M. W. Wanlass, K. A. Emery, T. A. Gessert, G. S. Horner, C. R. Osterwald and T. J. Coutts, *Sol. Cells, 27* (1989) 191.

13 D. Morel, K. Blaker, W. Bottenberg, L. Fabick, B. Felder, M. Gardenier, D. Kumamoto, D. Reinker and R. Rifai, *Proc. 8th E. C. Photovoltaic Solar Energy Conf., Florence, Italy, May 9–13, 1988*, Vol. 1, Kluwer, Dordrecht, 1988, pp. 661–670.

14 W. Bottenberg and D. Reinker, *Proc. 20th IEEE Photovoltaic Specialists Conf., Las Vegas, NV, September 26–30, 1988*, IEEE, New York, 1988, p. 1230.

15 T. Glatfelter, J. Burdick, J. Fournier and L. Boman, *Proc. 19th IEEE Photovoltaic Specialists Conf., New Orleans, LA, May 4–8, 1987*, IEEE, New York, 1987, pp. 194–199.

16 D. Morel, R. Wieting and K. Mitchell, *Technical Digest of the First International Photovoltaic Science and Engineering Conference, Kobe, Japan*, PVSEC-1, Tokyo, Japan, 1984, pp. 567–570.

17 D. L. King and R. B. Siegel, *Proc. 17th IEEE Photovoltaic Specialists Conf., Kissimmee, FL, May 1–4, 1984*, IEEE, New York, 1984, p. 944.